Diffusion-Controlled Startup of a Gas-Loaded Liquid-Metal Heat Pipe

R. Ponnappan*
Universal Energy Systems, Inc., Dayton, Ohio 45432
L. I. Boehman†
University of Dayton, Dayton, Ohio 45469
and
E. T. Mahefkey‡
Wright Research and Development Center, Wright-Patterson Air Force Base, Ohio 45433

Liquid-metal heat pipes have exhibited difficulties starting up from a frozen-state. Inert gas loading is a possible solution to the frozen-state startup problem. A few research papers give results of this technique. The applicability of the method to heat pipes with arterial grooves and long adiabatic lengths is unknown. The present study deals with the diffusion-controlled startup analysis and testing of an argon-loaded, 2-m-long, stainless steel-sodium heat pipe of the double-walled type with artery channel and long adiabatic section. A two-dimensional, quasisteady state, binary vapor-gas diffusion model determined the energy transport rate of vapor at the diffusion front. The analytical solution to the diffusion problem provided the vapor flux, which in turn was used in the one-dimensional transient thermal model of the heat pipe to predict the time rate of change of temperature and position of the hot front. The experimental test results successfully demonstrated the startup of a gas-loaded sodium heat pipe and validated the diffusion model of the startup.

Nomenclature

C = heat capacity per unit length of tube, wick and fluid, J/m · K
c = total molar density of mixture, kg · mole/m^3
c_c = c evaluated at temperature T_c
c_h = c evaluated at temperature T
c_i = initial molar density of the noncondensible gas, kg · mole/m^3
D = binary diffusion coefficient, m^2/s
D_o = outer diameter of outer tube, m
F_{HC} = radiation shape factor between hot and cold zones, unitless
g = dimensionless vapor flux (diffusion parameter), unitless
h_{fg} = heat of vaporization per unit mass, J/kg
ℓ = dimensionless length
L = length, m
M = total mass of fluid depleted, Eq. (33), kg
M_v = molecular weight of vapor
$\dot{m}$ = rate of fluid mass depletion during startup, Eq. (32), kg/s
N_g = molar gas flux, kg · mole/m^2 · s
N_i = initial vapor flux, kg · mole/m^2 · s
N_v = molar vapor flux, kg · mole/m^2 · s
P = pressure, Pa
P_i = initial pressure of noncondensible gas at room temperature, Torr
P_v = vapor pressure, Pa
q_i, q_o, q_r, q_v = reduced Q_i, Q_o, Q_r, Q_v, respectively, s^{-1}
Q = heat flow rate, W
Q_i = heat input rate, W
Q_o = heat rate radiated at the condenser, W
Q_r = heat rate exchanged between the hot and cold zones internally, W
Q_v = heat-transport rate of the vapor diffusing into the noncondensible gas at the vapor-gas front, W
R = universal gas constant, kJ/kg · mole K
r = radius, m
$\bar{r}$ = dimensionless r
r_v = vapor core radius, m
T = temperature, K
T_c = room temperature, K
T_s = test chamber shroud temperature, K
t = time, s
x_g = mole fraction of noncondensible gas, mole/mole
x_v = mole fraction of vapor, mole/mole
y = noncondensible gas concentration variable, Eq. (10), unitless
z = distance along pipe, m
$\bar{z}$ = dimensionless z
ϵ = emissivity
θ = dimensionless temperature, Eq. (21-24)
$\lambda(\theta,\ell)$ = parameter, Eq. (9)
σ = Stefan-Boltzmann constant, W/m^{2}K^4

Subscripts

A = adiabatic
C = condenser
E = evaporator
H = hot zone
P = pipe
v = vapor

Received March 28, 1989; revision received Oct. 5, 1989. This paper is declared a work of the U.S. Government and is not subject to copyright protection in the United States.

*Senior Scientist, Scientific Services Division. Member AIAA.
†Professor, Department of Mechanical Engineering. Member AIAA.
‡Deputy Chief, Aerospace Power Division, Aero Propulsion and Power Laboratory. Member AIAA.

Introduction

FUTURE space missions could require large-area space radiators constructed out of liquid metal heat pipes to reject large amounts of waste heat at rejection temperatures of 1000 K or more. Peak electric power, in excess of 1 MWe, is required and which generates waste heat in the form of pulses

with a peak-to-average ratio of 10^4–10^5 based on the mission and orbital duty cycles envisioned.[1] Essentially, these heat pipes have to withstand directed energy impacts or pulsed-heat input loads. A space nuclear-power system is a typical example of a power supply requiring such high-capacity liquid-metal heat pipes.[2] Another example is NASA's Space Station, designed to be powered by a solar dynamic power system which will require thermal energy storage and some form of energy transport device (liquid-metal heat pipe) for transporting energy to the power conversion unit.[3] The transition from illuminated to eclipse portion of the orbit will introduce transient thermal loads on the heat pipe device.[4] In addition, cold start or thawing of liquid-metal heat pipes is a unique problem for space or terrestrial applications. Uniform distribution of the working fluid within the heat-pipe wick structure is important during shutdown of any heat-pipe device. An abrupt shutdown during a dryout may cause irrecoverable damage.[5] Long transport lengths cause priming and flow-resistance problems. Although active methods such as electrical trace heating or prelaunch thawing can be adapted for startup, they are neither convenient nor desirable. A passive and reliable startup technique which will not require onboard electrical power is preferred. Researchers have recommended filling the heat pipe with noncondensible gas in order to make it start more readily.[6,7] But the applicability of this technique has not been proved with the heat pipe of the double-wall artery type, which has a long transport section without any screen wick. The objectives of the present study were to 1) develop an analytical model for the startup based on the binary vapor-gas diffusion theory and 2) verify the analytically predicted results with those of an experimental gas-loaded heat pipe especially designed and built for this purpose.

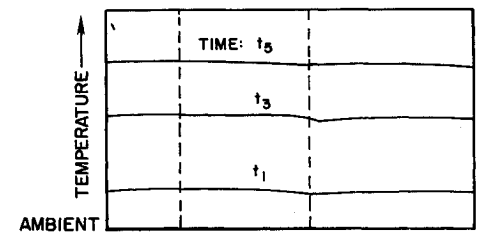

a) UNIFORM STARTUP

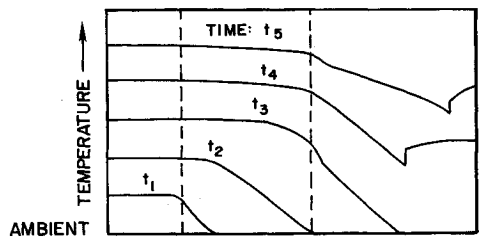

b) FRONTAL STARTUP (NO NONCONDENSIBLE GAS)

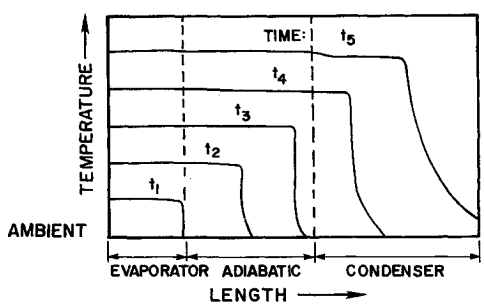

c) FRONTAL STARTUP (WITH NONCONDENSIBLE GAS)
NOTE: $t_5 > t_4 > t_3 > t_2 > t_1 > 0$

Fig. 1 Heat-pipe startup characteristics.

Theoretical Analysis of Startup

Background

Marcus[8] conducted an extensive investigation on the theory and design of room temperature, gas-loaded, variable-conductance heat pipes (VCHP). His study concentrated mainly on the steady-state theory. Sockol[6] presented a model for the rapid startup of a high-temperature, gas-loaded heat pipe. A two-dimensional analysis was used. Startup was not initiated until the vapor pressure P_v in the hot zone reached a value equal to the initial gas-charge pressure P_i. Sockol showed that at the beginning of startup, the diffusion rate was high and decreased exponentially to a very low value as steady state was approached. However, his analytical results were not verified with any experimental data. Bystrov et al.[9] presented the results of experimental studies of the startup of vacuum and of gas-loaded, sodium heat pipes by sudden and smooth application of heat to the evaporator. Bystrov and Goncharov[7] examined an approximate method of calculating the unsteady temperature fields and the startup characteristics for a quick startup and switching to the heat-pipe regime, using a lumped-parameter model for the vapor, predicted on a planar vapor-gas boundary. Their analytical results were in good agreement with the experimental results of an argon-filled, annular artery, sodium heat pipe without a transport section. Bobco[10] developed a closed-form expression for estimating the location of the minimum temperature in the inactive condenser of a VCHP under steady state. He presented equations to show how the gas-reservoir design may be based on the operating conditions for maximum heat load and incipient freezeout. El-Genk and Seo[11] developed a two-dimensional transient model capable of predicting the operating limits of liquid-metal heat pipes during steady-state and transient operations. Their model assumed a completely thawed heat pipe with no noncondensible gas in the vapor core of an annular wick heat pipe. Thus, the literature review for the related background research revealed very minimal coverage of the scope of the present study on diffusion-controlled startup of a gas-loaded, liquid-metal heat pipe.

Startup Characteristics

Startup characteristics for heat pipes are shown in Fig. 1. Heat pipes with working fluids (e.g., water, ammonia, etc.) having high vapor pressures at startup temperatures typically exhibit uniform startup, whereas those (e.g., sodium, potasium, etc.) with low vapor pressures exhibit frontal startup. Use of noncondesible gas (NCG) in the vapor core makes the startup front steeper (e.g., sodium heat pipe with argon). Elaborate details on the stages of frozen-state startup explaining the phase-change process and hydrodynamic events are available in the literature.[12–14] Generally, in the moderate temperature (122–628 K) VCHP research, Q_v has been reported to be much smaller than the axial conduction Q_{ax}, with the diffusion rate assumed constant.[8,10,14] For high-temperature heat pipes, Sockol[6] found that Q_v is much larger than Q_{ax} and that Q_v approaches Q_i at the beginning of the startup and drops to almost zero when steady state is approached. This theory justifies the stationary vapor-gas front of steady state.

Diffusion Model and Analysis

The objective of the diffusion analysis is to determine the vapor diffusion rate past the hot front as a function of the length and temperature of the hot zone. The model is based on Fick's law for a binary gas system explained in detail by Bird et al.[15] and developed by Sockol.[6]

The following *assumptions* are used in this analysis:

1) The local condensation rate upstream of the front is negligible.

2) The cold wall acts as a perfect sink for the vapor.

3) The transition region between the cold and hot zones is very thin.

4) The upstream vapor velocity is uniform over the cross section.

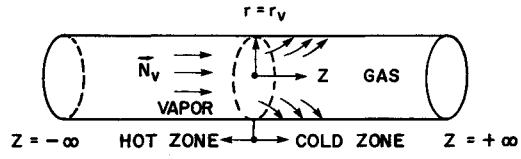

Fig. 2 Coordinate system for diffusion analysis.

5) The gas is stagnant throughout the pipe
6) The hot zone is nearly isothermal.
7) The vapor velocity during startup is limited to sonic speed.
8) In a long cylindrical heat pipe, the vapor concentration should relax to a quasisteady profile in time of order $(r_v/2.4)^2/D$. If the distance moved by the front during this time is small, steady-flow equations can be used for the diffusion analysis.[6] For the sodium-argon system at 1000 K, with $r_v = 0.635$ cm and $D = 4.591$ cm^2/s, the relaxation time is 15.25 ms. As will be seen in the numerical analysis results in a later section, the rate of front movement varies from 0.04–0.37 cm/s for a power input range of 100–1000 W with the gas-charge pressure of 0.2 Torr. Hence, the front movement in 15.25 ms is very small and the steady-state diffusion assumption is justified.
9) The diffusion coefficient D is evaluated at the average temperature of the hot and cold zones.

Fick's law for binary diffusion in the form of molar flux is given by Eq. (1).[15]

$$N_v = x_v(N_v + N_g) - cD_{vg}\nabla x_v \tag{1}$$

For a stagnant gas, $N = 0$ and the total mass fraction of the system, $x_g + x_v = 1$.

Applying the principle of conservation of mass applicable to the vapor flow, it can be shown that

$$\nabla^2 \ell n\, x_g = 0 \tag{2}$$

In order to solve this equation and to set up the necessary boundary conditions, a cylindrical coordinate system is introduced as shown in Fig. 2. According to assumption 3, the axial distance over which x_g departs from zero or one is small compared to the hot-zone or cold-zone lengths. From the location of the front, the boundaries of z are at $\pm\infty$. The boundary conditions are as follows:

$z<0$:

1) As $z\to-\infty$, the vapor flux N_v is given by an unknown constant flux N_i.

$$cD_{vg}\frac{\partial}{\partial z}(\ell n\, x_g)\to N_i, \qquad \text{as } z\to-\infty \tag{3}$$

2) At the wall, the vapor flux N_v in the radial direction is zero as there is no condensation in the hot zone.

$$\frac{\partial}{\partial r}(\ell n\, x_g) = 0, \qquad \text{at } r = r_v \tag{4}$$

$z>0$:

1) At the condenser end, there is no vapor; only gas exists.

$$x_g\to 1, \qquad \text{as } z\to+\infty \tag{5}$$

2) At the wall (perfect sink), there is no sodium vapor due to complete condensation $x_v = 0$ and $x_g = 1$

$$x_g = 1, \qquad \text{at } r = r_v \tag{6}$$

A mass balance on the gas is done to obtain the unknown vapor flux N_i in terms of the initial molar concentration c_i of the NCG at T_c.

$$\begin{bmatrix}\text{mass of}\\ \text{gas}\\ \text{in pipe}\end{bmatrix} = \begin{bmatrix}\text{mass of}\\ \text{gas}\\ \text{in hot zone}\end{bmatrix} + \begin{bmatrix}\text{mass of}\\ \text{gas}\\ \text{in cold zone}\end{bmatrix}$$

$$= \begin{bmatrix}\text{mass of}\\ \text{gas}\\ \text{in hot zone}\end{bmatrix} + \begin{bmatrix}\text{mass of}\\ \text{vapor + gas}\\ \text{in cold zone}\end{bmatrix} - \begin{bmatrix}\text{mass of}\\ \text{vapor}\\ \text{in cold zone}\end{bmatrix} \tag{7}$$

If the total length of the heat pipe is L_P and the hot-zone length is L, then Eq. (9) can be expressed in the integral form as

$$c_i L_P = c_h\int_{-\infty}^{0}\bar{x}_g\,dz + c_c(L_P - L) - c_c\int_0^{\infty}\overline{(1-x_g)}\,dz \tag{8}$$

where the bar indicates an average over the cross section.

From ideal gas law, the molar densities at various temperatures are expressed as

$$c_i = \frac{P_i}{RT_c}, \qquad c_c = \frac{P_v(T)}{RT_c}, \qquad c_h = \frac{P_v(T)}{RT}$$

Introduce dimensionless variables as follows:

$$\bar{r} = \frac{r}{r_v}, \qquad \bar{z} = \frac{z}{r_v}, \qquad \ell = \frac{L}{r_v}, \qquad \ell_P = \frac{L_P}{r_v} \tag{9a}$$

$$\theta = \frac{T}{T_c}, \qquad g = \frac{N_i r_v}{cD}\ \text{(diffusion parameter)} \tag{9b}$$

$$\lambda(\theta,\ell) = \frac{c_c(L_P - L) - c_i L_P}{c_c r_v} = \ell_P - \ell - \frac{\ell_P P_i}{P_v(T)} \tag{9c}$$

A new dependent variable y is introduced in place of $\ell n\, x_g$ as

$$y(\bar{r},\bar{z}) = -\frac{\ell n\, x_g}{g} \tag{10}$$

Equation (2) in cylindrical coordinates transforms to

$$\frac{1}{\bar{r}}\frac{\partial}{\partial\bar{r}}\left(\bar{r}\frac{\partial y}{\partial\bar{r}}\right) + \frac{\partial^2 y}{\partial\bar{z}^2} = 0 \tag{11}$$

Boundary conditions, Eqs. (3–6), become

$$\left.\begin{aligned} &\bar{z}<0: \frac{\partial y}{\partial\bar{z}}\to -1, && \text{as } \bar{z}\to-\infty\\ &\frac{\partial y}{\partial\bar{r}} = 0, && \text{at } \bar{r} = 1\\ &\bar{z}>0: y\to 0, && \text{as } \bar{z}\to\infty\\ &y = 0, && \text{at } \bar{r} = 1 \end{aligned}\right\} \tag{12}$$

Rearranging and normalizing Eq. (8),

$$\lambda(\theta,\ell) = \int_0^{\infty}\overline{(1-x_g)}\,d\bar{z} - \frac{c_h}{c_c}\int_{-\infty}^{0}\bar{x}_g\,d\bar{z} \tag{13}$$

Averaging the gas concentration over the cross section, and letting

$$F_c(g) = 2\int_0^1 \bar{r}\,d\bar{r}\int_0^{\infty}(1 - e^{-gy})\,d\bar{z} \tag{14}$$

$$F_h(g) = 2\int_0^1 \bar{r}\,d\bar{r}\int_{-\infty}^{0} e^{-gy}\,d\bar{z} \tag{15}$$

Eq. (13) becomes,

$$\lambda(\theta,\ell) = F_c(g) - (1/\theta)\, F_h(g) \tag{16}$$

Solution Method

The partial differential Eq. (11) and the boundary conditions Eq. (12) are solved for $y(\bar{r},\bar{z})$ in the closed form using Bessel functions as described by Sockol.[6] Once y is known, g can be obtained by solving Eq. (16). The mass flux in terms of θ and ℓ are obtained by performing the radial integral numerically. A simplifying approximation is used for this purpose. For large values of g, $F_h(g)$ is negligible compared to $F_c(g)$ and the radial integral yields

$$F_c(g) = (1/\beta_1)(\ln g - 1.339) \tag{17}$$

where $\beta_1 = 2.4048$ is computed from the zeros of Bessel function. Now, the approximate equation for $F_c(g)$ is

$$F_c(g) \approx \lambda(\theta,\ell) \approx (1/\beta_1)(\ln g - 1.339) \tag{18}$$

or

$$g = \exp(1.339 + \beta_1\lambda) \tag{19}$$

The energy transport by vapor diffusion from the hot to cold zone Q_v is given by

$$Q_v = \pi r_v^2 M_v N_i h_{fg} = \pi r_v M_v cDh_{fg} g \tag{20}$$

The values of cD for sodium-argon mixture as a function of temperature are computed from the kinetic theory of gases using the Chapman-Enskog[15] relation as $3.4\text{–}12.6 \times 10^{-6}$ g-moles/cm s in 300–1200 K. The diffusion parameter g has to be very large at the beginning of the startup in order to have large Q_v and must drop to zero toward the end of startup.

Transient Thermal Analysis

The transient state of the gas-loaded, liquid-metal heat pipe with a long adiabatic section at time t after the application of evaporator power input Q_i is shown in Fig. 3. Figure 3a shows the heat pipe during the thawing process when there is no heat output at the condenser. Figure 3b shows the condition when the pipe is transporting and radiating out Q_o at the condenser.

Assumptions

1) Axial conduction is negligible compared to Q_v during startup.

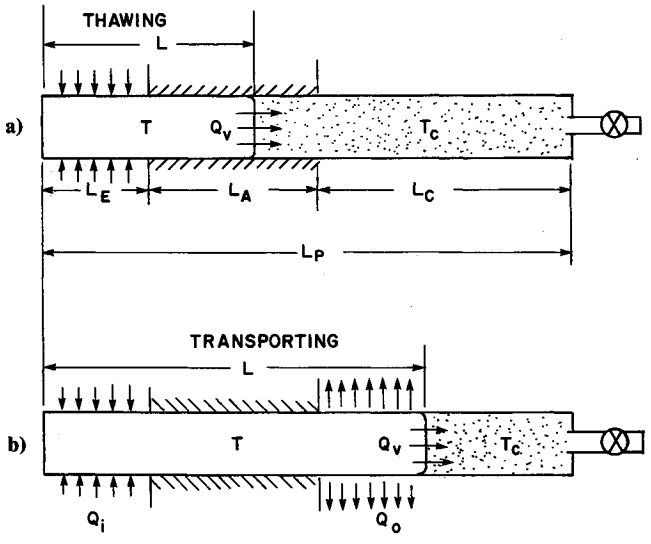

Fig. 3 Transient state of the heat pipe at time t during a) thawing and b) transporting.

2) The evaporator and adiabatic sections are insulated such that no heat loss occurs in the radial direction.

3) Axial and radial temperature variations within the same zone (hot or cold) are not considered. The hot zone is at a uniform temperature T and the cold zone (gas slug region) is uniformly at T_c. Only the time dependence of temperature and the location of the hot front are analyzed, i.e., $T = T(t)$; $L = L(t)$.

4) There is no liquid return flow to the evaporator during the thawing stage, and there is enough fluid inventory to last until the pipe starts up.

5) Initially, the wick structure is saturated with the working fluid, which is in a frozen state.

6) The heat-pipe vapor core is filled with an NCG (argon) charge at a pressure P_i and temperature T_c.

7) No chemical reaction occurs between the fluid and gas.

8) The mechanism of vapor diffusion into the gas within the vapor core is as outlined in the previous section.

9) Horizontal orientation of the pipe is assumed during startup.

10) Heat input to the evaporator is uniform along its length and it can be conductively or radiatively coupled, whereas the heat removal at the condenser is radiatively coupled to the cold sink at T_s.

11) The reservoir wick at the end of the evaporator is in good capillary contact with the evaporator wick.

12) The heat of fusion of sodium ($\sim$115 J/g) is neglected while thawing as it accounts for only 2% of the heat transport.

Definitions

1) *Initial hot-zone temperature or rise temperature* (T_{Hi}) is the temperature at which the sodium vapor pressure is equal to the adjusted initial NCG charge pressure P_i such that

$$P_v(T_{Hi}) = P_i\left(\frac{L_P}{L_P - L_E}\right)$$

2) *Startup temperature* (T_{Hs}) is the temperature of the hot zone when the hot front has reached the beginning of the condenser.

3) *Rise time* (t_i) is the time required to raise the temperature of the evaporator to T_{Hi} from T_c after the Q_i is applied.

4) *Startup time* (t_s) is the time taken after t_i for the hot front to move to the beginning of the condenser, i.e., to move through the adiabatic length L_A.

Governing Differential Equations

Energy balances are conducted for the control volumes enclosing the hot and cold zones of the heat pipe during the transient states of hot zone diffusing into the cold zone as depicted in Fig. 3. Two sets of equations corresponding to the thawing stage and transporting stage for each of the control volumes are written with the initial and boundary conditions. The equations are normalized using the following reduced variables:

$$\theta = \frac{T}{T_c}, \qquad \theta_s = \frac{T_s}{T_c}$$

$$\ell = \frac{L}{r_v}, \quad \ell_E = \frac{L_E}{r_v}, \quad \ell_A = \frac{L_A}{r_v}, \quad \ell_C = \frac{L_C}{r_v}, \quad \ell_P = \frac{L_P}{r_v}$$

$$q_i = \frac{Q_i}{C_E r_v T_c}, \qquad q_v = \frac{Q_v}{C_E r_v T_c}, \qquad q_r = \frac{Q_r}{C_E r_v T_c}$$

$$q_o = \frac{Q_o}{C_E r_v T_c}, \qquad s_1 = \frac{C_A}{C_E}, \qquad s_2 = \frac{C_C}{C_E}$$

The reduced equations and the boundary conditions are as follows:

$$[\ell_E + s_1(\ell - \ell_E)]\frac{d\theta}{dt} = q_i - q_v - q_r \tag{21}$$

Boundary condition: $\theta = 1$ at $t = 0$; for $0 < t < t_s$ and $\ell_E \le \ell \le (\ell_E + \ell_A)$.

$$[\ell_E + s_1\ell_A + s_2(\ell - \ell_E - \ell_A)]\frac{d\theta}{dt} = q_i - q_v - q_r - q_o \tag{22}$$

Boundary condition: $\ell = (\ell_E + \ell_A)$ at $t = t_s$; for $t_s < t < \infty$ and $(\ell_E + \ell_A) \le \ell \le \ell_P$.

$$s_1(\theta - 1)\frac{d\ell}{dt} = q_v \tag{23}$$

Boundary condition: $\ell_E = \ell$ at $t = 0$.

$$s_2(\theta - 1)\frac{d\ell}{dt} = q_v \tag{24}$$

Boundary condition: $\ell = (\ell_E + \ell_A)$ at $t = t_s$.

$$q_v = A_v g \tag{25a}$$

where

$$A_v = \frac{\pi M_v c D h_{fg}}{C_E T_c} \tag{25b}$$

Table 1 Input data for the program SODART for 2-m liquid-metal double wall artery heat pipe

Program input parameters	Input data
1. Vapor core radius r_v	0.635×10^{-2} m
2. Evaporator length, L_E	0.375 m
3. Adiabatic length, L_A	0.745 m
4. Condenser length, L_C	0.910 m
5. Total length, L_P	2.030 m
6. Evaporator unit thermal capacity, C_E	911.717 J/m K
7. Adiabatic unit thermal capacity, C_A	598.934 J/m K
8. Condenser unit thermal capacity, C_C	886.340 J/m K
9. Molecular weight of sodium, M_v	23
10. Emissivity of condenser surface, ϵ_P	0.66
11. Stefan-Boltzmann constant, σ	5.669×10^{-8} W/m^2 K^4
12. Emissivity of vapor core surface, ϵ_H	0.1
13. Shape factor between hot and cold zone, F_{HC}	0.01159
14. Room temperature, T_c	300 K
15. Chamber sink temperature, T_s	300 K
16. NCG charge pressure, P_i	0.05, 0.10, 0.20, 0.50, 1.00, 2.00 Torr
17. Evaporator input, Q_i	100, 250, 500, 1000 W
18. Solution stop time	3000 s

$$q_o = A_o(\ell - \ell_A - \ell_E)(\theta^4 - \theta_5^4) \tag{26a}$$

where

$$A_o = \frac{\pi D_o \epsilon_p \sigma T_c^3}{C_E} \tag{26b}$$

$$q_r = A_r \ell\,(\theta^4 - 1) \tag{27a}$$

where

$$A_r = \frac{2\pi r_v F_{HC} \epsilon_H \sigma T_c^3}{C_E} \tag{27b}$$

From the diffusion analysis, we have Eqs. (9) and (19) for $\lambda(\theta,\ell)$ and g. With this, the formulation of the transient problem is completed, and the numerical solution technique is described next.

Numerical Computations

The governing differential equations and the initial conditions, Eqs. (21-27), are solved by numerical integration using the fourth-order Runge-Kutta method for the 2-m sodium-argon experimental heat pipe. A FORTRAN program called SODART was developed for this purpose. The input data required for the program is given in Table 1. The temperature-dependent properties such as the diffusion coefficient cD and the enthalpy of vaporization h_{fg} are input as coarse table and interpolated within the program for fine intervals. Since $P_v(T)$ is an exponentially varying property, the empirical relation [Eq. (28)] by Ditchburn and Gilmour[16] is used.

$$P_v = 2.29 \times 10^{11}(T^{-0.5})(10^{-5567/T}) \tag{28}$$

where T is in degrees Kelvin and P_v in Newton/square meter.

Computation of Startup Parameters

The startup parameters are computed as follows. For the given P_i, the startup vapor pressure is found from

$$P_v(T_{Hi}) = P_i(T_c)\frac{L_P}{(L_P - L_E)} \tag{29}$$

From the sodium vapor pressure relation [Eq. (28)], T_{Hi} corresponding to $P_v(T_{Hi})$ is computed. Applying the energy conservation principle to the hot zone and neglecting the losses, one obtains the equations for t_i and t_s.

Table 2 Results of the startup analysis

Sl. No.	Startup parameters	Evaporator power input Q_i, W	Noncondensible gas initial charge pressure P_i, (Torr) 0.05	0.10	0.20	0.50	1.00	2.00
1	Rise time t_i, s	100	1076.8	1150.9	1230.7	1345.6	1440.7	1543.9
		250	430.7	460.4	492.3	538.2	576.3	617.6
		500	215.4	230.2	246.1	269.1	288.1	308.8
		1000	107.7	115.1	123.1	134.6	144.1	154.4
2	Startup time t_s, s	100	1563.0	1673.0	1791.0	1961.0	2105.0	2261.0
		250	625.0	669.0	715.0	783.0	841.0	903.0
		500	313.0	335.0	359.0	391.0	421.0	451.0
		1000	157.0	167.0	179.0	197.0	211.0	225.0
3	Rise temperature T_{Hi}, K	All Q_i	614.9	636.6	659.9	693.6	721.4	751.6
4	Startup temperature T_{Hs}, K	All Q_i	634.3	657.4	682.4	718.4	748.3	780.8
5	Sodium mass depletion M from the evaporator integrated over the startup time t_s s, g	All Q_i	32.9	35.3	38.0	41.7	45.1	48.5
6	Location L of hot front in 3000 s after rise time, m	100	1.317	1.291	1.267	1.238	1.218	1.200
		250	1.620	1.564	1.511	1.446	1.401	1.360
		500	1.901	1.846	1.784	1.695	1.626	1.560
		1000	2.011	1.999	1.980	1.935	1.886	1.882

$$t_i = \frac{Q_i}{C_E L_E (T_{Hi} - T_c)} \tag{30}$$

$$t_s = \frac{Q_i}{(C_E L_E + C_A L_A)(T_{Hs} - T_c)} - t_i \tag{31}$$

T_{Hs} is computed from the SODART program by solving the governing differential equations [Eqs. (21-27)].

During the time of thawing, vapor mass flow rate is governed by Q_v. If m is the rate of mass depletion in the evaporator during startup, Q_v can be written as

$$Q_v = \pi r_v^2 M_v N_i h_{fg} = \dot{m} h_{fg} \tag{32a}$$

or

$$\dot{m} = \frac{Q_v}{h_{fg}} \tag{32b}$$

By integrating $\dot{m}$ with respect to time, the total mass of sodium vaporized from the evaporator and transferred to the adiabatic section is obtained.

$$M = \int_0^{t_s} \dot{m}\, dt \tag{33}$$

This integration is automatically available from the Q_v computation in SODART.

Results of Computations

A matrix of computations was done varying the P_i and Q_i values. For every value of Q_i (i.e., 100, 250, 500, and 1000 W), six P_i values (0.05, 0.1, 0.2, 0.5, 1.0, 2.0 Torr) were varied, and a total of 24 computations was done. In each set of computations, the transient results t vs L, T, Q_v, Q_o, Q_r, and M were computed for 3000 s. The time step used was 10^{-3} s, and the CPU time consumed in a CDC mainframe computer was 220 s.

Table 2 lists the results of the startup parameters. It is observed that the parameters time, temperature, and mass increase with an increase in the NCG charge pressure P_i, while the location of the hot front decreases. The important design input variable for heat pipe operating condition in terms of selecting the NCG charge pressure is obtained from these results, i.e., the integrated sodium mass-depletion values. Only the mass-depletion value of 38.0 g for $P_i = 0.2$ Torr satisfied the design conditions (evaporator and reservoir wicks hold 38.23 g sodium); hence, this value of the charge pressure was recommended. This does not preclude experimentation at other charge pressures (0.05-2.0 Torr) provided 1) the frozen-state startup is not attempted at $P_i > 2.0$ Torr, 2) the heat pipe is overfilled with sodium, and 3) a partial evaporator dryout operation is tolerable. The 2.0-Torr limit was based on the 1000 K operating temperature limit and the need to minimize the gas-slugged condenser length during steady-state operations.

The major aspects of the transient results of the computation are presented in the graphs of Figs. 4-6, which correspond to a typical power input of $Q_i = 250$ W and show L vs t, T vs t, and Q_v or Q_o vs t, respectively. Similar graphs for other power inputs are easily obtainable. The general trend of the Q_v vs t curves (Fig. 6) is important. At the start, Q_v is as high as Q_i and as the hot front moves, Q_v drops exponentially to a very low value at the end. The kink in the curve where the slope changes signifies the abrupt change in the thermal capacity of the adiabatic to condenser section. On the other hand, Q_o remains zero until the hot front reaches the condenser and increases fast to a maximum toward the end. The variation of the hot-zone temperature is only marginal in Fig. 5. The rise temperature is nearly as high as the startup temperature, and this signifies the frontal nature of the startup. The hot-front length and temperature results are compared and corroborated with the experimental data in the results section.

Applicability of This Analysis to Other Heat Pipes

The present diffusion analysis for the frozen startup is applicable in general to any gas-loaded, liquid-metal heat pipe irrespective of its geometry or wick design. Noncircular cross sections can be reduced to equivalent circular cases for analysis purposes. Arteries must be gas tolerant. A few boundary conditions and heat-capacity values have to be changed if the

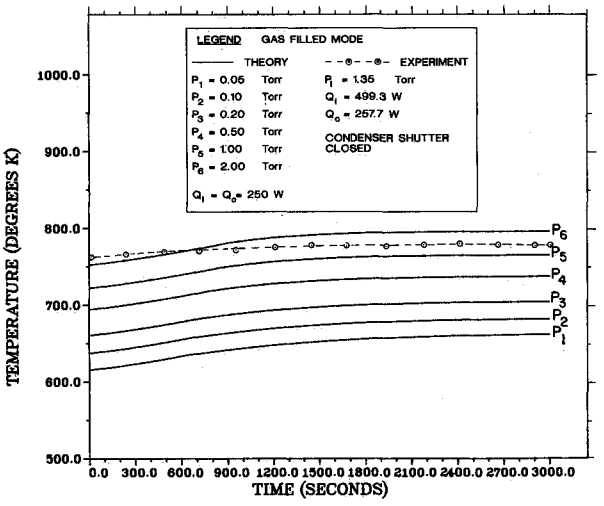

Fig. 5 Hot-zone temperature variation during startup; T vs t for $Q_o = 257.7$ W (Experiment) and 250 W (Theory).

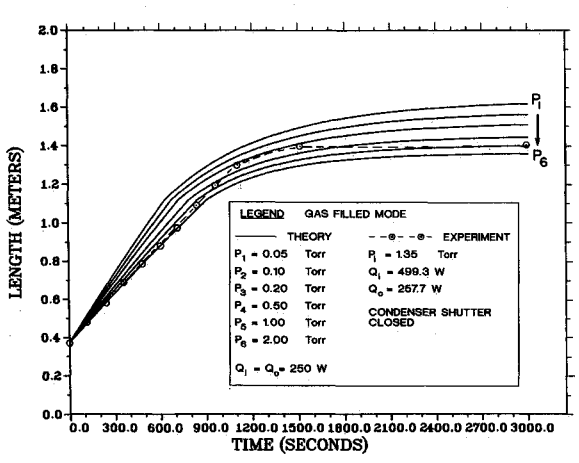

Fig. 4 Hot-zone length variation during startup; L vs t for $Q_o = 257.7$ W (Experiment) and 250 W (Theory).

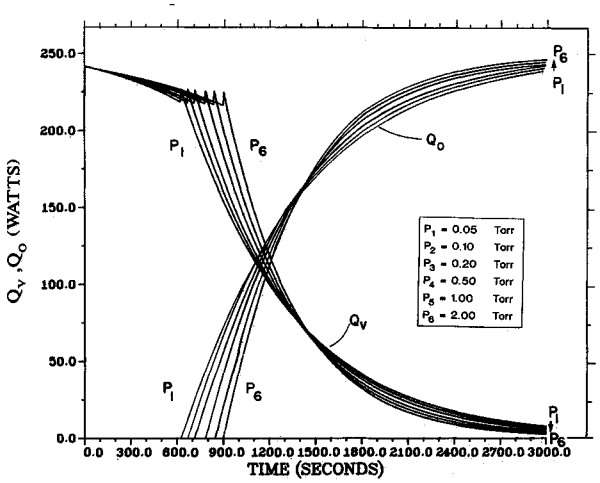

Fig. 6 Q_v and Q_o vs t for $Q_i = 250$ W (Theory).

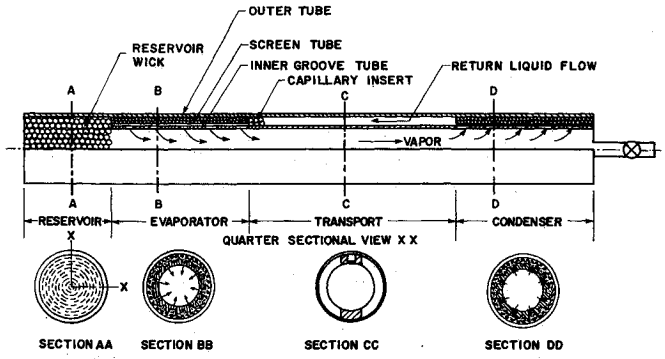

Fig. 7 Single-channel artery heat-pipe verification model.

transient thermal model [Eqs. (21-25)] is used for other designs. The double-wall artery is a special high-capacity design.[17] Its evaporator can handle high heat fluxes, and the transport section is entrainment free. As the frozen-startup problem is thus solved, the liquid-metal, double-wall heat pipe could be a potential candidate for high-temperature space radiators.

Experimental Work

The 2-m-long experimental heat pipe assembly consisted of an outer tube, an inner tube, two screen tubes, a reservoir screen plug, two end caps, a capillary insert plug, and a process valve with a fill tube as shown in Fig. 7. The pipe was vacuum baked at 1173 K and 10^{-7} Torr for 6 h before loading 93.4 g (22% overfill) sodium, by a gravity-aided vacuum-transfer method. The design summary of the heat pipe is available in Ref. 13. The heat pipe was instrumented with electrical resistance heaters and chromel-alumel thermocouples and mounted inside a vacuum chamber. Cooling water was circulated through the coil wrapped around the chamber for calorimetry. Figure 8 shows the schematic of the test setup. The heat pipe was tested in the horizontal position with the adiabatic artery at the 3 o'clock orientation. Startup and performance tests were conducted in the gas-filled mode with the initial charge pressure of 1.35 Torr. The recommended 0.2 Torr gas charge could not be obtained due to practical difficulties. Frozen-state startup tests were usually started in the beginning of the day when the pipe had cooled down to room temperature. A desired constant input power was applied to the evaporator, and the temperatures along the length of the heat pipe were recorded for 150 min at intervals of 2 min. Performance tests were done by allowing the transient tests to continue until a steady state was reached. At steady conditions, axial temperatures, power input, cooling water inlet and outlet temperatures, and flow rate were recorded.

Results and Discussion

The experimental heat pipe was first tested in vacuum mode for verifying the design performance and checking the calorimetric accuracy of the setup. It was then filled with 1.35 Torr argon at room temperature and tested for frozen-state startup characteristics. The repeatability and calorimetric test results were good. Only the gas-filled-mode test results are presented here. At low heat inputs (< 600 W), losses in the evaporator and adiabatic zones were higher than the transported energy which was less than 50%. At high inputs (>600 W), Q_o was stable at 55-60% of Q_i.

Axial Temperature Profile

Figure 9 shows the steady-state axial temperature profiles for various transported power levels (Q_o from 145-718 W). The adiabatic-zone temperatures are isothermal at each power level, and the position of the hot front lies at different axial locations in the condenser zone. The frontal nature of the temperature front is evident from this figure. The slant of the front is off-vertical, and the temperature of the cold zone is progressively high with increase in Q_o. This signifies the dominance of axial conduction over the diffusion mechanism at the steady-state condition where $Q_v = 0$.

Startup Temperature Profiles

Figure 10 shows the axial temperature profiles at 20, 30, 60, and 150 min after the application of power input. The temperature front at 20 min is in the adiabatic zone, and the profile of the front is relatively flatter than that in the condenser zone. At 150 min, the front is completely in the condenser zone and is more slanted. The vapor-diffusion activity is strong during the transient state, and the axial conduction is dominant in the steady state. Figure 11 shows the transient temperature profiles at a few specified axial locations for $Q_o = 257.7$ W. The number shown along each of the curves represents the thermocouple (T.C.) location. The rise time t_i for the given power level is obtained from this plot by finding the time (after power on) at which T.C. #4 attained a temperature close to the rise temperature T_{Hi} within 2 K. Also, the startup time t_s is obtained in a similar procedure applied to T.C. #11 and counting the time from the rise time. The startup temperature corresponds to the temperature T.C. #11 reached at the startup time. During startup, each T.C. location registers a sharp rise in temperature in the adiabatic zone and somewhat slow rise in the condenser zone due to the heat loss in that zone. The pipe started up from the frozen state for all power inputs up to $Q_i = 564$ W ($Q_o = 306$ W) when applied almost instantly. Beyond this power level, only gradual increments of 25 W were possible. In addition, the heater operating temperature limitation (1273 K) restricted the heat input level.

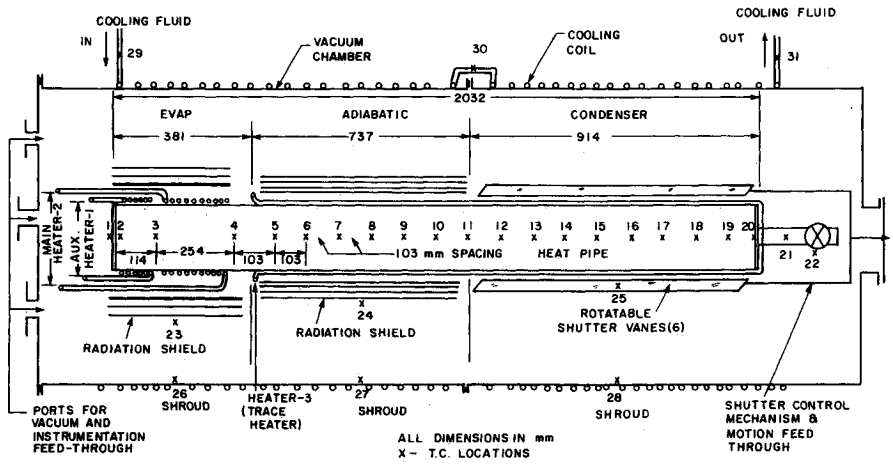

Fig. 8 Schematic diagram of the test setup.

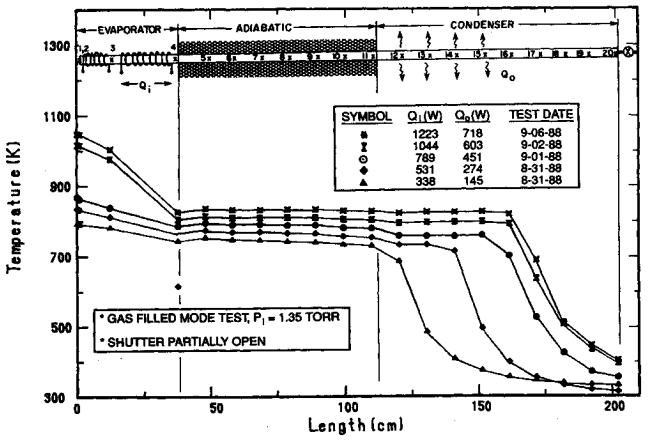

Fig. 9 Steady-state test axial temperature profiles (gas-filled mode).

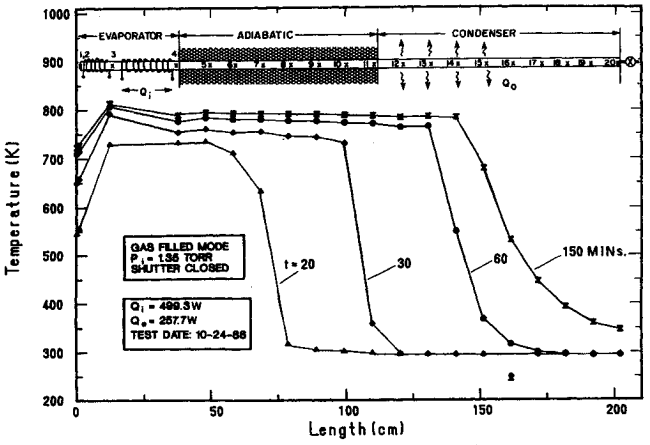

Fig. 10 Axial temperature profiles at specified time from 0–150 min after power input; T vs L for $Q_o = 257.7$ W.

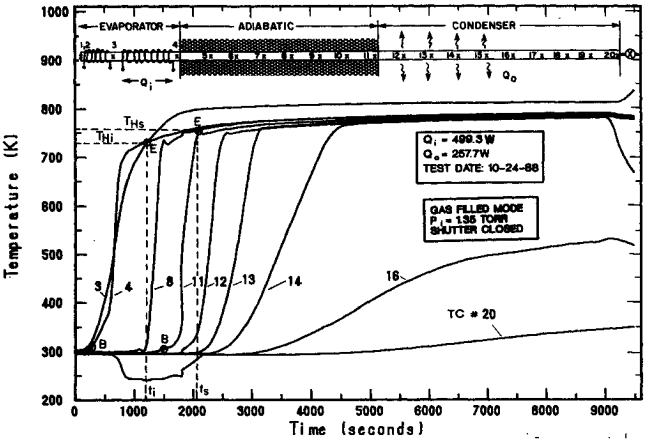

Fig. 11 Transient temperature profiles at specified axial locations; T vs t for $Q_o = 257.7$ W.

Hot-Front Propagation

The beginning of the heating process is marked by a sudden rise in temperature (designated as point "B" in Fig. 11), and the ending of the heating is marked by more or less constant temperature (variation within 2 K) designated by point "E" in Fig. 11. In the present work, the ending point "E" is taken as the reference to locate the hot front of the diffusing front. The "B" and "E" point designation applies to all of the thermocouple positions whether the slope of the temperature profile is steep or otherwise. However, the point "E" will not be applicable if a particular T.C. has not reached the startup temperature.

Table 3 Test results of startup parameters for $Q_o = 257.7$ W and $P_i = 1.35$ Torr

Startup parameters	Results: Theory	Results: Experiment
1. Rise time t_i, s	600	1200
2. Startup time t_s, s	875	840
3. Rise temperature T_{Hi}, K	735	732 ± 4.5
4. Startup temperature T_{Hs}, K	765	774 ± 4.5
5. Location L of hot front in 3000 s after rise time, cm	138	141 ± 5

Figure 4 shows the comparison of the experimental results with the analytical predictions for $Q_o = 257.7$ W. The agreement between the experimental and analytical results is good. It may be observed that the experimental points lie along a mean theoretical curve between $P_i = 1.0$ and 2.0 Torr. The small deviation is attributed to the limitations of length determination (± 0.05 m uncertainty) and temperature measurement (± 4.5 K uncertainty).

Hot-Zone Temperature Variation

The experimental temperature variation of the hot zone is plotted for $Q_o = 257.7$ W in Fig. 5. The experimental data match fairly the theoretically calculated values. All of the points lie along the $P_i = 1.0$ to 2.0 Torr band of the theoretical curves. In the time axis, $t = 0$ corresponds to the rise time t_i. The 3000 s of transient test are counted after the lapse of t_i.

Startup Parameters

Table 3 gives the experimental values of these parameters. The experimental rise time is higher than that predicted because of unaccounted thermal mass of the heater coil, supports, and clamps attached to the evaporator and the neglect of heat of fusion of sodium during thawing. All of the other parameters match closely with the theory.

Conclusions

1) Noncondensible gas loading of the liquid-metal heat pipe helped the pipe to start easily even from the frozen state. Large power inputs (>600 W), if suddenly applied, caused evaporator dryout. The gas-charge pressure could be predetermined to minimize the inactive condenser length.

2) The long adiabatic artery without a fine capillary surface did not pose any priming problem in the presence of noncondensible gas.

3) In the gas-loaded mode, the heat-front propagation during startup was found to be solely diffusion controlled, whereas in the steady state, axial conduction determined the temperature profile of the front. The axial conduction rate accounted for approximately 15 W which was only 2–10% of the condenser radiated power.

4) The variable-conductance feature would be an added benefit of the startup solution if needed for operational reasons.

5) The theoretical predictions of the rise time, rise temperature, startup time, startup temperature, heat front vs time plot, and hot-zone temperature vs time plot and experimental verification were in good agreement.

6) The computational time required for the transient predictions was small.

Acknowledgments

This research was conducted at the Aero Propulsion and Power Laboratory of the Wright Research and Development Center. Technical services by J. Tennant, D. Ryan [Universal Energy Systems (UES)] and D. Reinmuller (Aero Propulsion and Power Laboratory) and publications help by UES staff are appreciated and acknowledged.

References

[1]Mahefkey, E. T., "Overview of Thermal Management Issues for Advanced Military Space Nuclear Reactor Power Systems," *Space Nuclear Power Systems 1984,* Vol. 2, edited by M. S. El Genk and M. D. Hoover, Orbit, Malabar, FL, 1985, pp. 405-407.

[2]Ranken, W. A., "Heat Pipe Development for the Spar Space Power System," *Advances in Heat Pipe Technology,* edited by D. A., Reay, Pergamon, London, 1982, pp. 561-574.

[3]Keddy, E., Sena, J. T., and Merrigan, M., "Development of an Integrated Heat-Pipe Thermal Storage System for a Solar Receiver," AIAA Paper 88-2683, June 1988.

[4]Hendricks, R. C., Simoneau, R. J., and Dunning, J. W., Jr., "Heat Transfer in Space Power and Propulsion Systems," *Mechanical Engineering,* Vol. 108, Feb. 1986, pp. 41-52.

[5]Merrigan, M. A., "Heat-Pipe Technology Issues," *Space Nuclear Power Systems 1984,* Vol. 2, edited by M. S. El Genk and M. D. Hoover, Orbit, Malabar, FL, 1985, pp. 419-426.

[6]Sockol, P. M., "Startup Analysis for a High-Temperature Gas-Loaded Heat Pipe," NASA-TM-X-2840, July 1973.

[7]Bystrov, P. I., and Goncharov, V. F., "Starting Dynamics of High-Temperature Gas-Filled Heat Pipes," *High Temperature (USA),* Vol. 21, No. 6, 1983, pp. 929-936.

[8]Marcus, B. D., "Theory and Design of Variable Conductance Heat Pipes," NASA CR-2018, April 1972.

[9]Bystrov, P. I., Goncharov, V. F., Kharchenko, V. N., and Shul'ts, A. N., "Transient Heat and Mass Transfer in Liquid-Metal Pipes," *Heat Transfer—Soviet Research (USA),* Vol. 14, No. 3, 1982, pp. 18-23.

[10]Bobco, R. P., "Variable Conductance Heat Pipes: A First-Order Model," *Journal of Thermophysics and Heat Transfer,* Vol. 1, No. 1, 1987, pp.35-42.

[11]El-Genk, M. S. , and Seo, J. T., "A Transient Model for Liquid-Metal Heat Pipes," *Transactions of the 5th Symposium on Space Nuclear Power Systems,* Institute for Space Nuclear Power Studies, Univ. of New Mexico, Albuquerque, NM, 1988.

[12]Ivanovskii, M. N., Sorokin, V. P., and Yagodkin, I. V., *The Physical Principles of Heat Pipes,* translated by R. Berman and G. Rice, Clarendon, Oxford, UK, 1982.

[13]Ponnappan, R., "Studies on the Startup Transients and Performance of a Gas-Loaded Sodium Heat Pipe," Ph.D. Dissertation, Univ. of Dayton, Dayton, OH, Dec. 1988.

[14]Chi, S. W., *Heat-Pipe Theory and Practice: A Source Book,* McGraw-Hill, New York, 1976.

[15]Bird, R. B., Stewart, W. E., and Lightfoot, E. N., *Transport Phenomena,* Wiley, New York, 1960.

[16]Sittig, Marshall, *Sodium—Its Manufacture Properties and Uses,* Reinhold, New York, 1956.

[17]Ponnappan, R., Beam, J. E., and Mahefkey, "Improved Double-Wall Artery High Capacity Heat Pipe," *Journal of Spacecraft and Rockets,* Vol. 22, No. 6, 1985, pp. 592-597.